Flow In a Circular Pipe Filled With Porous Medium in the non-Darcian Effects

السريان في وسط مسامي دائري تحت التأثيرات اللادارسيه

M.S. El-Kady, M.A. Tolba and L.H. Rabie

Power Mechanical Engineering Department
Mansoura University, Egypt

خلاصـــــه:

في هذا البحث دراسة عدديه ومعمليه للسريان في مجرى دائري مملوء بوسط مسامي. حيث إستخدمت معادلة كميه الحركة التفاضليه للسريان في وسط مسامي بصورتها العامة والتي تشتمل على التأثيرات اللادارسيه المختلفة مثل المسامية المتغيرة، القصور الذاتي للمائع والاحتكاك اللزج عند الحوائط. تم حل المعادلة التفاضليه لكمية الحركة باستخدام طريقه الفروق البسيطة. أجريت الدراسة النظرية على وسط مسامي ذو حبيبات كرويه بأقطار $3 \le d \le 8$ مم، ونسبه قطر الحبيبات الكرويه الى نصف قطر المجرى الدائري $0.05 \le D \le 2.0$، وقد تم دراسة السريان في الوسط المسامي حتى رقم رينولدز Re يصل الى 10^5، ومعامل إنحدار الضغط B يصل الى 10^6. وأظهرت النتائج ان التأثيرات اللادارسيه لها تأثيرا واضحا على شكل توزيع السرعة في مقطع المجرى، وقد ظهرت هذه التأثيرات بشكل واضح في المناطق الملاصقة للحوائط وأعطتها زيادة كبيره في قيمه السرعة مما عمق من اندفاع سريان المائع في هذه المناطق. كما أعطى بالتبعية تأثيرا ملحوظا على خصائص السريان مثل معامل الاحتكاك اللزج وكذلك معامل الاحتكاك الناتج من تأثير المسامية (المسمى بانخفاض الضغط لدارسي) والاحتكاك الناتج من القصور الذاتي ومن ثم على معامل الاحتكاك الكلي. وقد أفادت النتائج ان المتغيرات المختلفة مثل قطر الكريات المكونه للوسط المسامي "d" ونسبه قطر الحبيبات الكرويه الى نصف قطر المجرى "D" ورقم دارسي المعدل Da ومعامل رينولد للسريان "Re" لها تأثيرا كبيرا على معامل الاحتكاك الكلي وعلى مكوناته الثلاثه. وقد أوضح تحليل النتائج التوافق الممتاز لمعامل الاحتكاك الكلي كدالة في رقم رينولدز مع معادله أيرجون Eurgon وذلك باستخدام معامل التفاذيه المتوسطه ε_m بدلا من معامل التفاذيه الفعال ε_e لحساب كل من معامل الاحتكاك ورقم رينولدز في محاور أيرجون Eurgon.

$$f_m = 175 / \mathrm{Re}_m + 1.75$$

كما أجريت دراسة معمليه على سريان مائع (ماء) في وسط مسامي مكون من أنبوبة دائرية المقطع ومحشوة بكرات من الصلب بأقطار مختلفه $3.2,\ 4,\ 4.7,\ 5.3,\ 6.3$ mm وأجريت مقارنه مع النتائج العددية أظهرت تطابقا جيدا أثبتت صحة هذا النموذج.

Abstract:

Forced flow through a circular pipe filled with saturated porous media has been numerically simulated. The generalized form of the momentum equation including the non-Darcian effects such as the variable porosity, flow inertia, and viscous friction is considered. To solve the momentum equation, the finite difference method is used. Different sphere diameters of $3 \le d \le 8$ mm, and sphere diameter to the pipe radius ratio

"D" in the range $0.05 \le D \le 2$ are considered. The results are obtained for flow Reynolds number up to 10^5, and nondimensional pressure gradient B up to 10^8. The results show that the non-Darcian effects have a significant influence on the velocity profiles. These effects appear clearly in the regions near to the wall and gives an increase in the magnitude of the velocity and signifies the channeling effect. It has in turns a significant influence on the fluid flow characteristics such as the boundary frictional drag, the frictional drag induced by the solid matrix (designed as Darcy's pressure drop) and the flow inertia drag and in turns in the total drag coefficient. The results show the great influence of sphere diameter d, sphere diameter to the pipe radius ratio D, Darcy number Da and the Reynolds number on the total drag coefficient f_t and also on the behavior of its three components. The predicted results of the total friction as function of Reynolds number exhibit excellent agreement with Ergun equation based on the area mean porosity ε_m instead of the free porosity ε_e. It confirms the fact that Ergun equation is also valid for porous media of ideutical spherical particles for the laminar, transient and turbulent regimes.

$$f_m = 175 / \mathrm{Re}_m + 1.75$$

To verify the numerical results, an experimental investigation was carried out for the flow of water in a circular tube filled with five different steel spheres of diameters 3.2, 4, 4.7, 5.4 and 6.3 mm respectively. Comparison with predicted results shows a very good agreement, and proves the validity of the model.

1. Introduction

Fluid flow in a porous media has been of continuous interest for the past five decades. This interest stems from the complicated phenomena associated with the flow process in porous media, and its very wide applications available. Such applications can be found in agriculture, chemical engineering, environmental protection, material science, thermal insulation, grain and coal storage, underground water hydrology, soil mechanics, drying technology, transpiration cooling, solid matrix heat exchanger, ceramic processing, catalytic reactors, and food processing technology. Consequently, understanding the associated transport processes is of critical importance.

The majority of the existing studies are pertinent to the fluid flow and heat transfer in porous media based on the Darcy flow model. The theoretical work of Vafia and Tien [1] attempted to account for boundary and inertial effects on forced convective flow in porous media. Vafia [2] and Vafia et al. [3] studied the effects of flow channeling on forced convection along a flat plate theoretically and experimentally. Kaviany [4] investigated a laminar flow through porous medium bounded by isothermal parallel plates with the Brinkman-extended flow model and constant matrix porosity and Nakayama et al. [5] treated the wall by a constant heat flux and peripherally uniform wall temperature. Polikakos and Renken [6] analyzed theoretically the forced flow in a channel filled with porous medium, and accounted for the effects of flow inertia, variable porosity, and Brinkman friction. But they did not

study these effects on the fluid flow characteristics. El Kady [7] investigated theoretically the forced convection heat transfer and flow in an annular channel filled with porous media taking into consideration the non Darcian effects. Cheng, et al. [8] analyzed the forced convection in the entrance region of a packed channel with asymmetric heating. The variable porosity close to an impermeable boundary has been reported by a number of investigators such as Benenati and Brosilow [9]. They show a distinct porosity variation in packed beds. Their results show a high porosity region close to the external boundary. Chandrasekhara and Vortmeyer [10] used the measurements of Benenati and Brosilow [9] to solve numerically for the velocity profile in isothermal packed beds. Wang and Du [11] analyzed experimentally the forced convective heat transfer in a vertical annulus filled with porous media. Amiri and Vafia [12] simulate numerically the forced convective incompressible flow through porous media, and the associated transport processes.

The existing literature on the fluid flow through porous media (packed sphere beds), give very limited quantitative information on the influence of considering the non-Darcian effects such as the variable porosity, flow inertia, and viscous friction on the fluid flow characteristics. It is the objective of this paper to provide an analysis for the flow through a circular pipe filled with saturated porous media (packed sphere beds), taking into consideration the variable porosity, flow inertia, and viscous friction and see its significant influence on the fluid flow characteristics such as the boundary frictional drag, the bulk frictional drag induced by the solid matrix (designed as Darcy's pressure drop) and the flow inertia drag induced by the solid matrix at high flow rates (designed as Forschheimer's form drag).

2. Mathematical Formulation

In order to formulate the problem, a steady, hydrodynamically fully developed fluid flow in a horizontal circular pipe filled with packed spheres as a porous medium is considered. It is assumed that the fluid and the solid matrix are in local thermal equilibrium and that the magnitudes of the physical properties such as the viscosity and density are constant. The physical configuration of the problem is shown in Figure (1).

Under these assumptions and by treating the solid matrix and the fluid as a continuum, the improved Darcy momentum equation including the viscous boundary friction and inertia effects are used:

$$1/\rho \,.\, [\,\partial P / \partial x] = \upsilon / r \,.\, [\partial / \partial r \,(\, r \;\partial u / \partial r)] - \upsilon\, u / \gamma - A\; u^2 \qquad (1)$$

where, u, P, ρ, υ are the velocity in the axial direction x, the pressure, the fluid density and the fluid dynamic viscosity respectively. γ and A are the permeability and the inertia coefficient (Forschheimer function) of the porous medium and are dependent on the porosity ε and other geometrical parameters of the medium. These parameters

are given by Ergun [13] for backed beds of identical spherical beads of diameter d and porosity ε as;

$$\gamma = d^2 \varepsilon^3 / [175 (1-\varepsilon)^2] \qquad (2)$$

$$A = 1.75 (1-\varepsilon) / [d \varepsilon^3] \qquad (3)$$

The present approach using equation (1) can be used from $\gamma \rightarrow 0$ (Darcian flow) to $\gamma \rightarrow \infty$ (Pure fluid flow). The first, second, and third terms on the right hand side of equation (1) are expressions for the boundary viscous drag which was introduced first by Brinkman [14], Darcy frictional drag which is responsible for the porous structure and inertia drag.

Due to the fact that, the particle diameter to the pipe radius ratio "D" is large enough, the porosity variation near the wall in no longer negligible. Therefore, it is assumed that the porosity "ε" varies exponentially from the wall. The experimental results of Benenati and Brosilow [9] for the porosity variation which is used later by Vafia et.al [3], Poulikakos and Renken [6], and Mularidhar and Kulacki [15] can be represented in the following form:

$$\varepsilon = \varepsilon_e [1 + b \exp(c.y/d)] \qquad (4)$$

Where y is the distance from the boundary wall, ε_e is the free stream porosity, and the empirical constants b and c are dependent on the particle diameter.

Numerical predictions were carried out for a porous media formed by spheres of diameter 3, 5, 6 and 8 mm. The constants chosen to represent the variation of ε_e, b, and c are similar to that used by Benenati and Brosilow [9] and Chandrasekhara and Vortmeyer [10] and El kady [7] among others. In the cases of d =3, 5 mm the values of the parameters are ε_e = 0.37, b = 0.35 and 0.43 and c= 3. For d = 8 mm, in the other hand, the values of the parameters are ε_e = 0.37, b = 0.9 and c = 2. For the case of d = 6 mm, the following values are assumed ε_e = 0.37, b = 0.53 and c= 3.

The boundary conditions imposed on the physical system are uniform with respect to the axial coordinate, the computational domain thus comprises of one half of the pipe over which the velocity u = 0 at $r = r_o$.

Using the dimensionless variables $U = u/u_m$, $R = r/r_o$ and $D = d/r_o$, the momentum equation (1) can be transformed to nondimensional form as:

$$U + C_1 . [Re/2] . U^2 = (B.\Gamma) . [2/Re] + (\Gamma/R) . [\partial / \partial R (R . \partial U / \partial R)] \qquad (5)$$

where, $C_1 = 0.01 D / (1-\varepsilon)$,

$\Gamma = \gamma / r_o^2 = D^2 \varepsilon^3 / [175 (1-\varepsilon)^2]$,

$Re = 2 u_m . r_o / \upsilon$, and

$$B = - \partial P / \partial x \, . \, [r_o^3 / \rho \upsilon^2]$$

u_m is the averaged fluid velocity including the solid and fluid regions and B is the nondimensional pressure gradient.

3. Fluid Flow Characteristics

The boundary frictional drag represents an overall characteristics of the channel flow, it is determined by the friction coefficient which is defined as [16-17] ;

$$f_v = \tau_w / [1/2 \, . \, \rho u_f^2] \qquad (6)$$

where τ_w is the mean wall shear stress and
u_f is the average local average velocity in the x-direction in void volume

In addition to the boundary frictional drag, the flow through the porous duct experiences also a bulk frictional drag induced by the solid matrix (designed as Darcy's pressure drop) and a flow inertia drag induced by the solid matrix at high flow rate (designed as Forschheimer's form drag). The bulk friction (Darcy) and the inertia (Forschheimer) drag coefficient and the total bulk drag which is the summation of the three drag types are defined [16-17] after changing the variables to our notations and definitions as follows:

$$f_D = \mu \, \gamma_m^{-1} \varepsilon_m \, u_f \, (r_o/2) / [\tfrac{1}{2} \rho u_f^2] \qquad (7)$$

$$f_i = 0.143 \, \rho \, \gamma_m^{-0.5} \varepsilon_m^{0.5} \, u_f^2 \, (r_o/2) / [\tfrac{1}{2} \rho u_f^2] \qquad (8)$$

$$f_t = - (dP/dx) \, (r_o/2) / [\tfrac{1}{2} \, \rho u_f^2] \qquad (9)$$

where γ_m is the permeability based on the area mean porosity ε_m

ε_m is the area mean porosity $\varepsilon_m = [1/r_o^2] \, . \int_0^{r_o} 2 \, r \, \varepsilon \, dr$

Equations (6) - (9) can be written as a function of the nondimensional parameters as:

$$f_v = 4 \, (dU/dR)\big|_{r_o} / Re_f \qquad (10)$$

$$f_D = \tfrac{1}{2} \, Da^{-1} / Re_f \qquad (11)$$

$$f_i = 0.0715 \, Da^{-0.5} \qquad (12)$$

$$f_t = f_v + f_D + f_i = 4 \, B / Re_f^2 \qquad (13)$$

where Da is the modified Darcy number $= \gamma_m / (4 \, r_o^2 \, \varepsilon_m)$
Re_f is the Reynolds number based of the velocity u_f, $Re_f = 2 \, u_f \, r_o / \upsilon$

In the present study equations (10) - (13) are used.

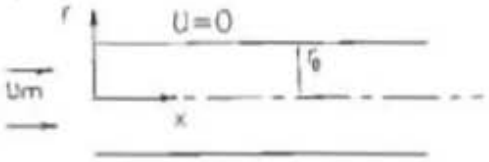

Fig. 1 Physical model, Coordinate system and boundaries

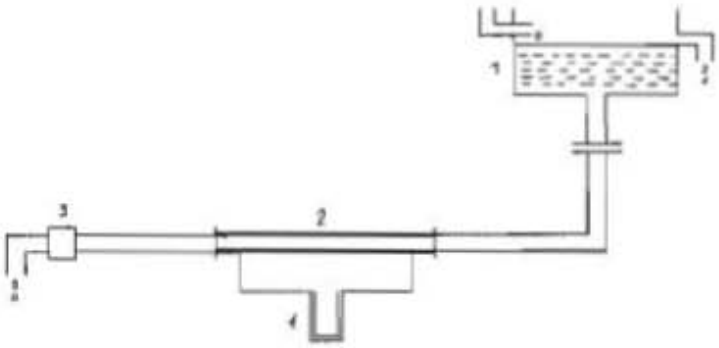

1. Overhead tank
2. Test section
3. Flow meter
4. U-tube manometer

Fig. 2 Schematic diagram of the experimental apparatus

4. Method of Solution

Finite difference equation is derived from equation (5). Both the first and second order derivatives were discretized by using central difference formulas [18]. The Forschheimer nonlinear term is linearized by guessing initial values of the velocity field at all the grid points, and the nonlinear term was written as the product of the unknown velocity and the guessed velocity. The difference algebraic equation is solved using the Gauss-elimination method [19] to yield the velocity field. A variable grid for accurate resolution of the important near-wall region is used in the Y-direction to obtain the momentum equation finite difference form.

5. The Experimental Work:

To validate the program developed for this study an experimental study for the flow in a porous media is carried out. A schematic diagram of the test rig is shown in Fig. 2. The test section is made of a copper tube of 20 mm inside diameter, and a 250 mm long. The tube is filled uniformly with stainless steel spheres of uniform sizes to form a backed bed to serve as the solid porous matrix through which fluid flows. The steel spheres are held in place by means of wire mesh located at the two ends of the tube. Five different sphere diameters are used through out this work. They are 3.2, 4.0, 4.7, 5.4 and 6.3 mm in diameter respectively. Fluid flows under the gravity action from a constant head tank 6.0 m above the test section. The porous section is kept horizontal in the gravitational open flow system. A calibrated orifice-meter is used as a flowmeter to measure the flow rate and from which the mean velocity and Reynolds number of the flow were calculated. A U-tube mercury manometer is connected to two pressure taps located just upstream and downstream the test section to measure the pressure drop along the test section. During the experiments the flow rate varied from 9.42×10^{-6} to 166×10^{-6} m^3/s. The experiments were performed carefully, each time the experiments were initiated at the largest flow rates; the objective was to produce a stable packing of the beads and to prevent the effects of changing porosity on the pressure drop as the flow rate was varied.

6. Results and Discussion

6.1 Flow velocity and Channeling

The Velocity distribution across the pipe flow in a porous media exhibit a channeling effect near the wall. It is considered the main driver for the behavior of the flow characteristics in such flow types. In order to give good explanations for the effect of the different geometric parameters such as the bead diameter d and its ratio to the pipe radius D on the flow characteristics, the velocity distribution and the channeling effect were studied.

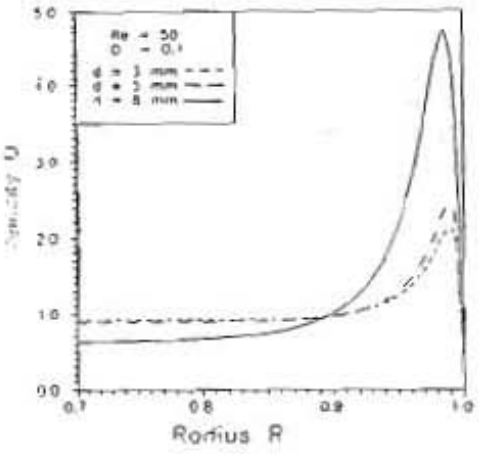

Fig. 3 Velocity distribution across the channel half width for different values of bead diameter d, $D = 0.1$ and Re=50

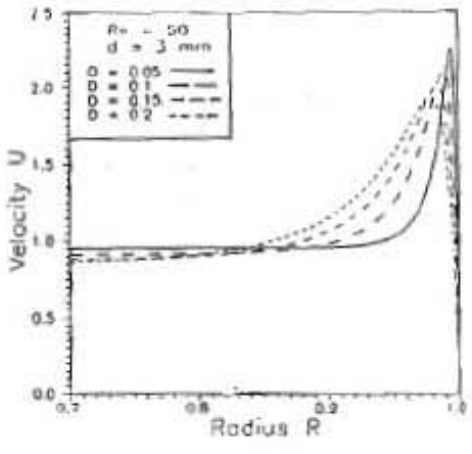

Fig. 4 Flow Velocity distribution across the channel half width for different values of D, $d = 3$ mm and Re=50

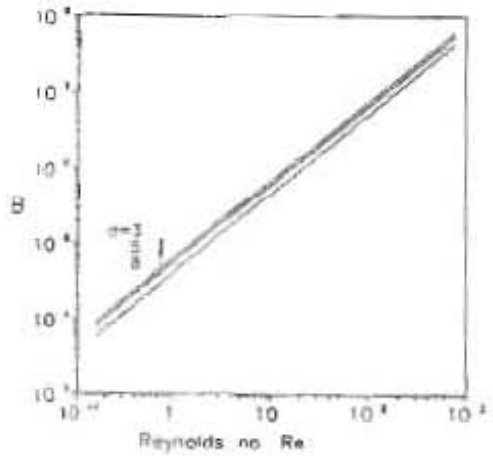

Fig. 5 Dependence of the pressure drop B on Re for different values of bead diameter d and $D = 0.1$

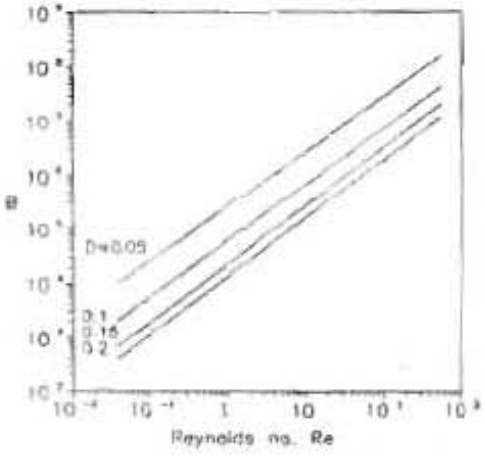

Fig. 6 Dependence of B on Re for a host values of bead diameter to channel radius D and $d = 3$mm

The dependence of the flow velocity and the channeling effect across the pipe half section on the bead diameter d and its ratio to the channel radius D are shown in Figs. 3 and 4. Fig. 3 shows the velocity distribution for the flow in a porous media of different sphere diameters d = 3, 5, and 8 mm, D = 0.1 and Re = 50. Fig. 4 shows the velocity distribution for the flow in porous media of different sphere to pipe diameters ratio D ($0.05 \leq D \leq .2$), d=3 mm and Re = 50. Both Figures show that with the increase of either d or D the permeability near the wall increases which in turns increases the channeling flow area near the wall.

6.2 Flow characteristics

The fluid flow is characterized by the friction factors f_v, f_d, f_i and f_t which are described by equations (10 -13).

The total friction factor f_t depends mainly on both Reynolds number and the nondimensional pressure gradient B. To show the effect of the different geometrical parameters on f_t it is very useful to know first the relation between both Re and B. Figs. 5 and 6 show the behavior of the nondimensional pressure gradient B with the change of Reynolds number for different values of d and D. Both Figures show the linear relation between B and Re in the logarithmic scale. The results show an increase in B with the increase of Re and its decrease with the increase of either the bead diameter d or the ratio D at constant Reynolds number.

Fig. 7 represents the variation of the total friction factor f_t with Re for d =3, 5 and 8 mm at constant D = 0.25. The total friction f_t decreases with the increase of the bead diameter. For constant Reynolds number the pressure gradient B decreases with the increase of the bead diameter as shown in Fig. 6 which leads to the increase of f_t. Fig. 8 shows the variation of the total friction factor f_t with Re for a range of the bead diameter to the tube radius ratio $0.05 \leq D \leq 1$. With the increase of D the nondimensional pressure gradient B decreases as shown in Fig. 6 which yields the decrease of the total friction factor f_t with the increase of Re and D. In Figs 7 and 8, the (f_t-Re) curves take the linearly shape in the laminar region, curved shape in the transient and constant value for the turbulent regions.

The behavior of the boundary viscous drag f_v, the Darcy friction f_D, inertia friction f_i and the total drag f_t with Reynolds number Re_f are presented in fig. 9 for d = 3 mm, D = 0.1 and in fig. 10 for d = 5.4 mm and D = 0.54. It is shown in Fig. 9 that the inertia friction factor f_i is independent on Re_f, while the Darcy friction factor f_D changes linearly in the logarithmic graph with Re_f. The values of f_i exceed the values of f_v when Re_f >65 and exceed the values of f_D when Re_f > 300. The curve of f_t assymptotes with the lines of f_D in the linearly shape laminar region and it assymptotes with the line of f_i in the constant value region where $Re_f > 5 \times 10^4$. In fig. 10 where bigger void area exists for the case of d = 5.4 and D = 0.54, the same trend of the data of the friction factors is observed but with smaller values.

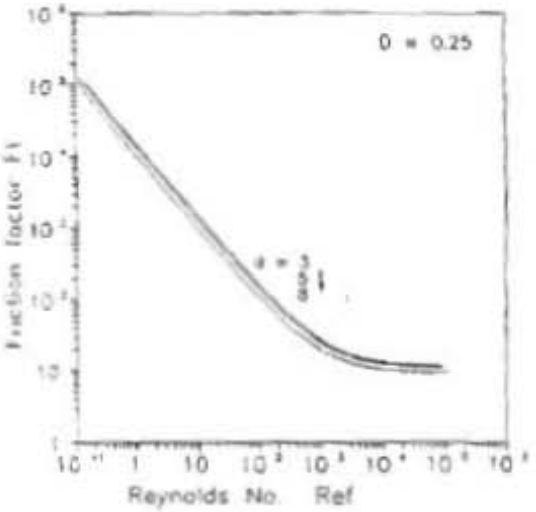

Fig. 7 total friction factor f_t variation with Re_f for d =3,5 and 8 mm and D=0.25

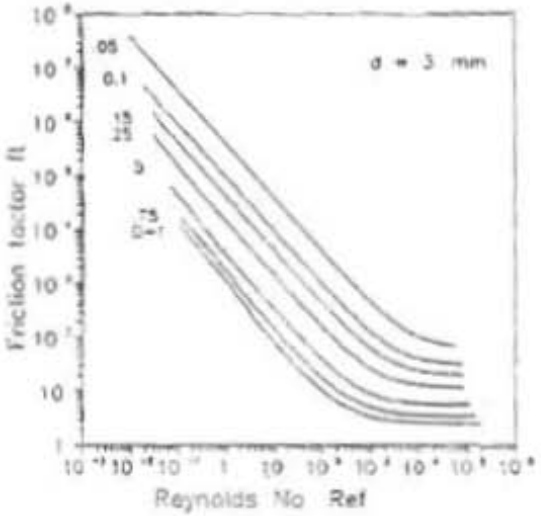

Fig. 8 total friction factor f_t variation with Re_f for a host of D values and d= 3 mm

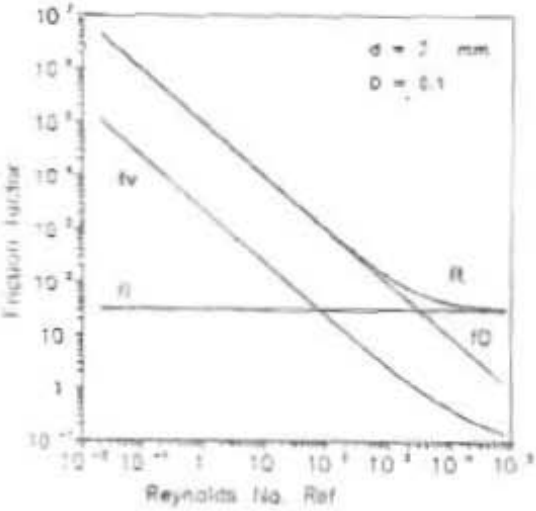

Fig. 9 friction factors f_t, f_D, f_v, f_i variation with Re_f for d = 3 mm and D = 0.1

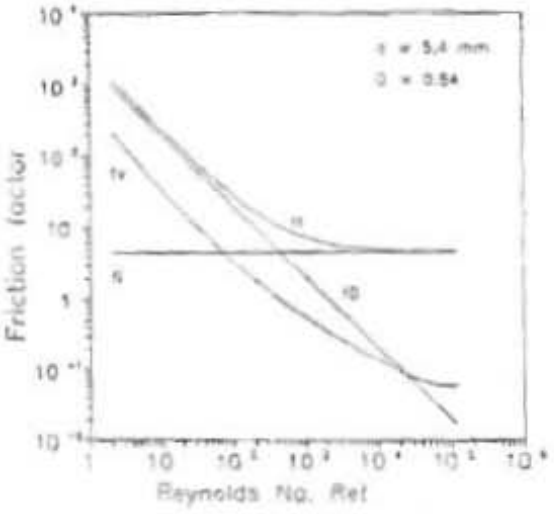

Fig. 10 friction factors f_t, f_D, f_v, f_i variation with Re_f for d = 5.4 mm and D = 0.54

Fig. 11 presents the relative sharing of each of the different friction factors in the total friction. It represents the values of f_D/f_t, f_v/f_t and f_i/f_t for $d = 3$ mm and $D = 0.1$, 0.25 and 0.5. With the increase of D i.e. the increase of the void volume, the values of the Darcy friction f_D/f_t decreases while both the inertia and viscous friction factors f_v/f_t and f_i/f_t increases. For $Re_f > 5x10^4$ both the Darcy and viscous friction f_D/f_t , f_v/f_t can be neglected, while the inertia friction f_i/f_t forms the main part of the total friction. For $Re_f < 100$ both the friction factors f_v/f_t and f_i/f_t are nearly constants but the Darcy friction f_D/f_t contributes the main part of the total friction. Fig. 12 gives the same relations shown in Fig. 11 but for more void media, for $d = 5.4$ mm and $D = 0.54$. The same trend appears with higher values of f_v/f_t and f_i/f_t but the Darcy friction f_D/f_t takes smaller values than that of the dense porous media presented in Fig. 11.

Fig. 13 illustrates the effect of Darcy number on the product of friction factor and Reynolds number. The total friction factor $f_t\,Re_f$, boundary friction $f_v\,Re_f$, Darcy's friction factor $f_D\,Re_f$, and Forschheimer's friction factor $f_i\,Re_f$, are plotted over the range $60 \le Da^{-1} \le 10^6$. It is seen that the value of $f_D\,Re_f$ exceeds $f_v\,Re_f$ when the value $Da^{-1} > 120$, the curve of $f_t\,Re_f$ overlaps with the lines of $f_D\,Re_f$ for $Da^{-1} > 5x10^4$. For $Da^{-1} \le 1$ Darcy friction $f_D\,Re_f$ and Forschheimer's inertia friction factor $f_i\,Re_f$ are almost negligible and the flow behaves just like the Posseuille flow. The results of parallel plates of Nakayama et al [5] and of the square channel of Hwang et al [17] are also represented with these results in Fig. 13 for comparison. A similar trend is observed between the data of parallel plates, the square channel and the circular channel.

It is more convenient to cast one relation to include the effects of the porosity variation and the sphere diameter. So, it is more suitable to plot the total friction factor versus Reynolds number in the nondimentional Ergun coordinates. In these coordinates the total friction factor and Reynolds number are based on the sphere diameter d and the free stream porosity ε_e and are defined as

$$f_e = (dP/dx)\ (d/2)\ [\varepsilon_e^3 / (1-\varepsilon_e)] \ /\ [1/2\ .\ \rho\ u_m^2] \qquad (14)$$

$$Re_d = u_m d / \upsilon\ .\ [1 / (1-\varepsilon_e)] \qquad (15)$$

The relation between f_e and Re_d is known as Ergun equation and represents the flow in laminar, transition and turbulent regimes. It fits available experimental data in fluid flows very well, (Ergun [13] and Rabie et al [20]). It is used for beds of small randomly unspherical beads as:

$$f_e = 175 / Re_d + 1.75 \qquad (16)$$

Figure 14 represents the relation of f_e versus Re_d for $d = 3$ mm and the different cases presented in Fig. 11 for $D = 0.05$, 0.15, 0.25, 0.5, 0.66, 0.75, and 1.0. Figure 14 shows that such presentation of results made all the data to collapse on nearly one curve. Comparing these results with those reported by Ergun and represented by the

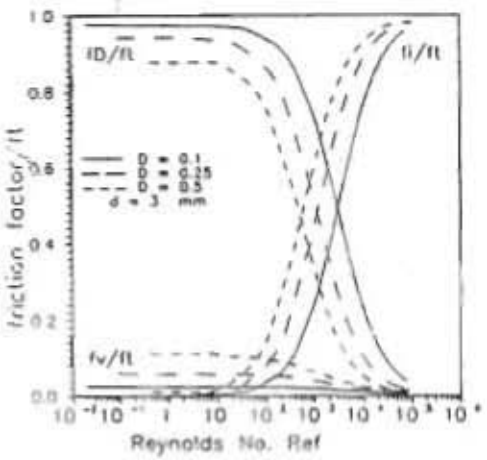

Fig. 11 friction factors f_D/f_t, f_v/f_t and f_i/f_t variation with Re_f for $d = 3$ mm and $D = 0.1$

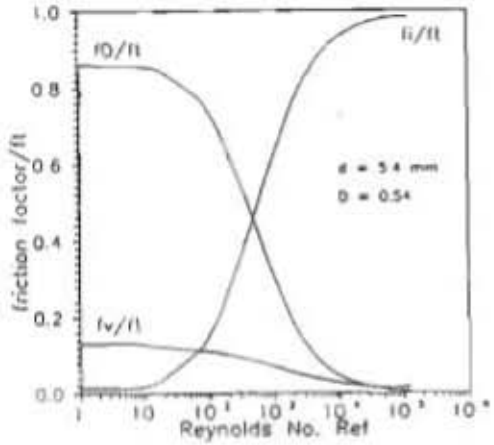

Fig.12 friction factors f_D/f_t, f_v/f_t and f_i/f_t variation with Re_f for $d = 5.4$ mm and $D = 0.54$

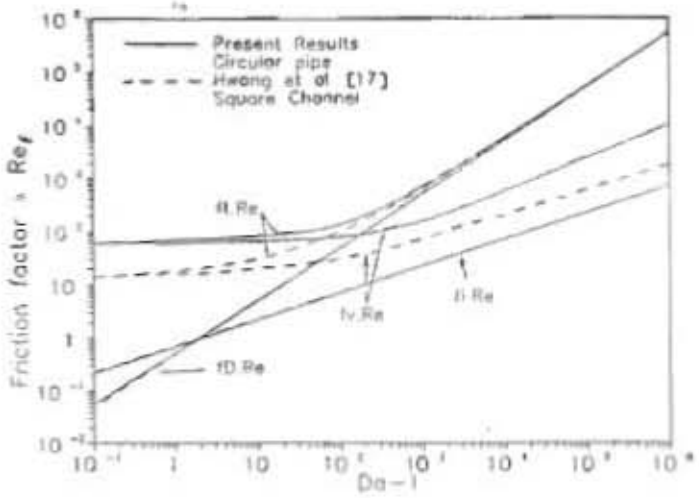

Fig. 13 $f.Re_f$ versus Da^{-1} for the present case and comparison with Hwang et al [17] for the square channel

empirical formula (16) for the identical spherical beads shows good agreement for the cases which have low values of the ratio of bead sphere diameter to the pipe outer radius, mainly $D = 0.05$ and $D = 0.15$. For higher values of D the data deviates from the Ergun curve. The deviation increases with the increase of D. The reason for such deviation may be attributed the channeling effect which is caused by the porosity variation near the wall and the higher velocity occurred there. For small values of D the channeling effect is small and the free stream porosity ε_e tends to equal the area mean porosity ε_m, therefore, the deviation in this case is very small. By the increase of D the porosity variation near the wall and the channeling effects increase. Therefore, the free stream porosity ε_e becomes more less than the area mean porosity ε_m and the deviation increases.

Defining f_m and Re_m as the total friction factor and Reynolds number based on the area mean porosity ε_m instead of the free porosity ε_e, a modified form of Ergun equation for the identical spherical beads can be casted from both variables f_m and Re_m.

$$f_m = 175 / Re_m + 1.75 \qquad (17)$$

Using the previous definitions in equations (17) the data of Fig. 14 can be represented in modified Ergun coordinates. Fig. 15 presents the relation between f_m versus Re_m for $d = 3$ mm and the different cases presented in Figs. 11 and 12 for $D = 0.05$, 0.15, 0.25, 0.5, 0.66, 0.75, and 1. Fig. 16 presents the relation between f_m versus Re_m for $D = 0.1$ and different bead diameters $d = 3$, 5, 6 and 8 mm. Such new presentation of results made all the data to collapse on one curve. This curve shows an excellent agreement with those results reported by Equation (17) for all the presented cases of D and d and for the laminar, transient and turbulent regimes. This result confirms the fact that Ergun equation can also be valid for porous media of identical spherical particles but with Reynolds number and the total friction factor based on the area mean porosity ε_m instead of the free porosity ε_e.

To validate the numerical model experimental test series were carried out. In which both the pressure drop and the volume flow rate were recorded and both Reynolds number and the total friction factor based on the area mean porosity ε_m were calculated and compared with the numerical results. Fig. 17 presents the comparison between the experimental and numerical values of the total friction factor with the change of Reynolds number for five spherical sized packed beads of 3.2, 4, 4.7, 5.4 and 6.3 mm diameter. The comparison shows good agreement of the presented results and proves the validity of the model.

7. Conclusions

In the present study, the generalized momentum differential equation including the non-Darcian effects such as the variable porosity, flow inertia and Brinkman viscous friction are solved by a numerical finite difference scheme to determine the flow

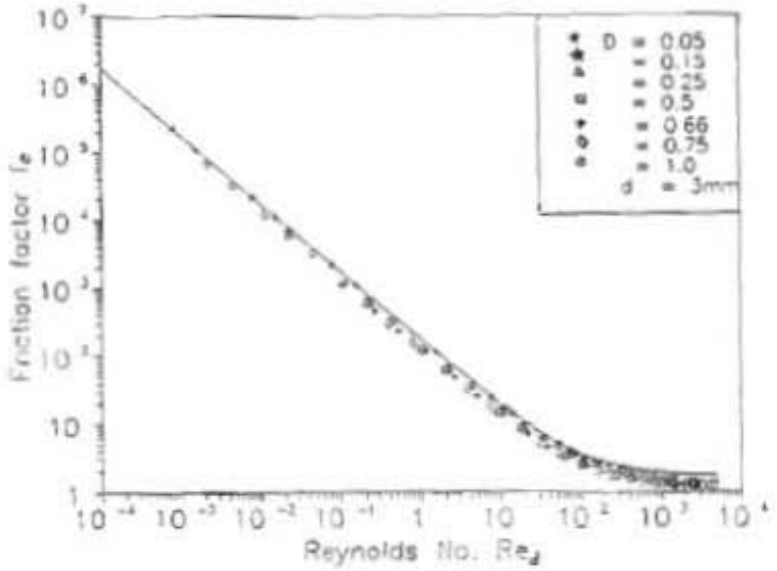

Fig. 14 total fiction factor f_d variation with Re_d for a host of D values and d=3mm

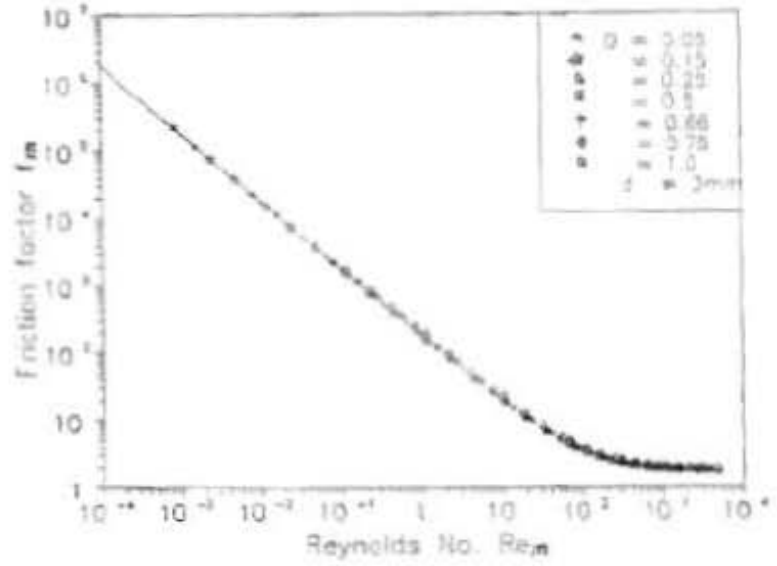

Fig. 15 total friction factor f_m variation with Re_m for a host of D values and d=3mm

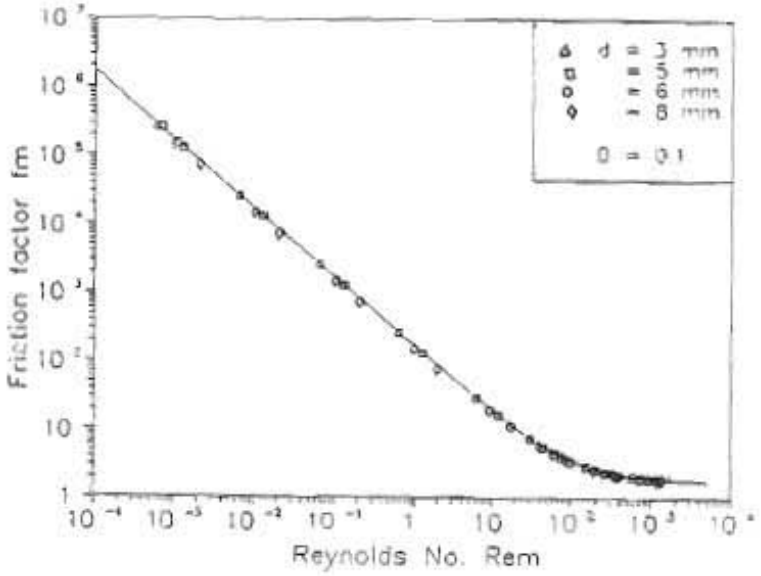

Fig. 16 total friction factor f_m variation with Re_m for $D = 0.1$ and $d = 3, 5, 6$ and 8mm

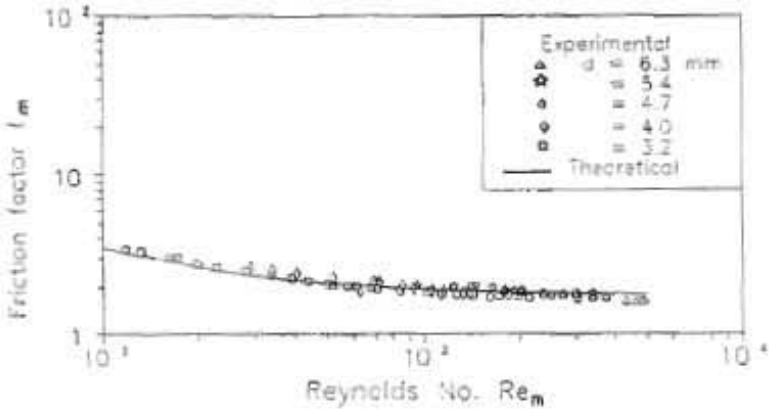

Fig.17 Total friction factor f_m versus Reynolds number. Comparison with the experimental results

characteristics in a circular pipe filled with porous material. The following conclusions can be made:

The variable porosity effect appears clearly in the regions near the walls only. It gives an increase in the velocity and signifies the channeling effect. Both the velocity and the channeling effect increase with the increase of the bead diameter, the ratio of bead diameter to channel radius D, or the increase of the nondimensional pressure gradient B.

The nondimensional pressure gradient B shows a linear relation in a logarithmic scale with Reynolds number Re. B increases with the increase of Re and decreases with the increase of either the bead diameter d or the ratio D at constant Reynolds number.

The total friction f_t curve takes the straight line shape in the laminar region, curved shape in the transient and constant shape for the turbulent regions. Its value decreases with the increase of the bead diameter, Re and the ratio of bead diameter to pipe radius D.

The inertia friction factor f_i is independent on Re_f, while the Darcy friction factor f_D changes linearly in the logarithmic graph with Re_f. The curve of f_i assymptotes with the lines of f_D in the linearly shape laminar region where both the friction factors f_i/f_t and f_v/f_t are nearly constants and very small while the Darcy friction f_D/f_t contributes the main part of the total friction. The curve of f_t assymptotes with the line of f_i for constant value region and both the Darcy and viscous friction f_D/f_t, f_v/f_t can be neglected, while the inertia friction f_i/f_t forms the main part of the total friction.

Ergun equation for the non-spherical particles porous media is also valid for porous media of identical spherical particles for the laminar, transient and turbulent regimes when both Reynolds number and total friction factor are based on the area mean porosity ε_m instead of the free porosity ε_e.

8. Nomenclature

A	Forschheimer inertia coefficient of the porous medium, equation 2
b, c	constants, equation 5
B	nondimensional pressure gradient , equation 7
C_1	dimensionless coefficients, equation 7
d	sphere diameter, mm
D	dimensionless sphere diameter = d/r_0
Da	modified Darcy number = $\gamma_m/(4r_0^2.\varepsilon_m)$
f_D	frictional drag factor induced by the solid matrix (Darcy's pressure drop and the flow inertia drag)

f_e	the total drag (friction) factor due to Ergun equation (14)
f_i	flow inertia drag induced by the solid matrix at high flow rate (designed as Forschheimer's form drag).
f_m	the total drag (friction) factor due to Ergun definition but based on ε_m
f_t	the total drag (friction) factor
f_v	the boundary viscous friction factor
P	pressure, Pa
r	radial coordinate
r_o	pipe radius
R	dimensionless radial coordinate
Re	Reynolds no. based on the tube diameter $Re = 2u_m \cdot r_o / \upsilon$
Re_d	Reynolds no. based on the bead diameter and ε_e, $Re_d = u_m \cdot d/\upsilon \cdot [1/(1-\varepsilon_e)]$
Re_f	Reynolds number based of the velocity u_f, $Re_f = 2\, u_f \cdot r_o / \upsilon$
Re_m	Reynolds no. based on the tube diameter and ε_m, $Re_m = u_m \cdot d/\upsilon \cdot [1/(1-\varepsilon_m)]$
u	field velocities in the x direction, m/s
U	non-dimensional field velocities in the X direction = u / u_m
u_f	local average velocity in the x-direction in void volume = u_m/ε_m
u_m	local averaged fluid velocity including the solid and fluid regions
x	axial coordinate
y	the distance from the pipe wall
γ	permeability of the porous layer, equation 2, m^2
γ_m	permeability based on the area mean porosity ε_m
Γ^*	dimensionless coefficients, equation 7.
ε	porosity of the porous medium
ε_e	free-stream porosity
ε_m	area mean porosity
τ_w	mean wall shear stress
υ	kinematic viscosity of the fluid, m^2/s
ρ	fluid density, kg/m^3

9. References

1. Vafia, K., and Tien, C. L., "Boundary and Inertia Effects on Flow and Heat Transfer in Porous Media," Int. J. Heat Mass Transfer, Vol. 24, pp. 195-203, 1981.
2. Vafia, K., "Convective Flow and Heat Transfer in Variable porosity Media," J. of Fluid Mechanics, Vol. 147, pp. 233-259, 1984.
3. Vafia, K., Alkire, R. L., and Tien, C. L., " An Experimental Investigation of Heat Transfer in Variable Porosity Media," ASME Journal of Heat Transfer, Vol. 107, pp. 642-647, 1985.
4. Kaviany, M., "Laminar Flow Through a Porous Channel Bounded by Isothermal Parallel Plates," Int. J. of Heat and Mass Transfer, Vol. 28, pp. 851-858, 1985.

5. Nakayama, A., Koyama, H., and Kuwaha, F., "An Analysis of Forced Convection in a Channel Filled With a Brinkman-Darcy Porous Medium; Exact and Approximation Solutions," Wärme und Stoffübertragung, Vol. 23, pp. 291-295, 1988.
6. Poulikakos, D., and Renken, K., "Forced Convection in a Channel Filled With Porous Medium, Including the Effects of Flow Inertia, variable Porosity, and Brinkman Friction," ASME, Journal of Heat Transfer, Vol. 109, pp. 880-888, 1987
7. El Kady, M., "Forced Convection Heat Transfer and Flow in an Annular Porous Medium in the Non-Darcian Effects" Mansoura Engineering Journal (MEJ), Vol. 19, No. 4, December 1994, pp. - .
8. Cheng, P., Hsu, C. T., and Chowdhury, A., "Forced Convection in the Entrance Region of a Packed Channel With Asymmetric Heating," ASME Journal of Heat Transfer, Vol. 110, pp. 946-954, 1988.
9. Benenati, R. F., and Brosilow, C. B., "Void fraction distribution in Packed Beds," AICHE J., Vol. 8, pp. 359-361, 1962.
10. Chandrasekhara, B. C., and Vortmeyer, D., "Flow Model for Velocity Distribution in Fixed Porous Beds Under Isothermal Conditions," Th.. Fluid Dynamics, Vol. 12, pp. 105-111, 1979.
11. Wang, B. and Du, J., "Forced convective heat transfer in a vertical annulus filled with porous media" Int. J. of Heat and Mass Transfer, Vol. 36, No. 17, pp. 4207-4213, 1993
12. Amiri, A. and Vafia, K., "Analysis of dispersion effects and non-thermal equilibrium, non-Darcian, variable porosity incompressible flow through porous media" Int. J. of Heat and Mass Transfer, Vol. 37, No. 6, pp. 939-954, 1994
13. Ergun, S., "Fluid flow through packed columns" Chemical Engineering Progress, Vol. 48, pp. 89-94, 1952.
14. Cheng, P.," Heat Transfer in Geothermal Systems," Advances in Heat Transfer, Vol. 14, pp. 1-105, 1979.
15. Muralidhar, K., and Kulacki, F. A.," Non-Darcy Natural Convection in a Saturated Horizontal Porous Annulus," ASME Heat Transfer Division, HTD Vol. 56 "Natural Convection in Porous Media", pp. 23-31, 1987
16. Chou, F. and Hwang, G., " Vorticity-Velocity method for the Graetz problem and the effect of natural convection in a horizontal rectangular channel with uniform wall heat flux" ASME J. of Heat Transfer, Vol. 109, pp. 704-710, 1987
17. Hwang, G., and Chao, C., " Effects of wall conduction and Darcy Number on laminar mixed convection in a horizontal square porous channel" ASME J. of Heat Transfer, Vol. 114, pp. 614-621, 1992.
18. Hirsch, C., "Numerical Computation of Internal and External Flows, Vol. 1: Fundamentals of Numerical Discretization" John Wiley & Sons , 1991.
19. Patankar, S., "Numerical Heat Transfer and Fluid Flow" Mc Graw Hill, New York, 1980.
20. Rabie, L. H., Arid, F. F., and Shalaby, M. A., " Flow of Dilute polymer solutions in porous media" Mansoura Engineering Journal, MEJ Vol. 11, No. 2, December 1986